INTERNATIONAL ATOMIC ENERGY AGENCY
UNITED NATIONS EDUCATIONAL, SCIENTIFIC AND CULTURAL ORGANIZATION

INTERNATIONAL CENTRE FOR THEORETICAL PHYSICS
34100 TRIESTE (ITALY) - P.O.B. 586 - MIRAMARE - STRADA COSTIERA 11 - TELEPHONE: 2240-1
CABLE: CENTRATOM - TELEX 460392-1

H4.SMR/285 - 6

WINTER COLLEGE ON
LASER PHYSICS: SEMICONDUCTOR LASERS
AND INTEGRATED OPTICS

(22 February - 11 March 1988)

THE THEORY & PRACTICE OF LATERAL-EFFECT POSITION-SENSITIVE SILICON PHOTODETECTOR

P.K. Buah-Bassuah
Istituto Nazionale di Ottica
Firenze, Italy

**

WINTER COLLEGE ON LASER PHYSICS: SEMICONDUCTOR LASERS AND INTEGRATED OPTICS.

at

(International Centre for Theoretical Physics, Trieste - Italy)

22 February - 11 March, 1988

THE THEORY AND PRACTICE OF LATERAL-EFFECT POSITION-SENSITIVE SILICON PHOTODETECTOR.

P.K. Buah-Bassuah[(a)], M. Melozzi[(b)], G. Longobardi

Istituto Nazionale di Ottica, Largo Enrico Fermi 6, 50125 Firenze

Italy

THE THEORY AND PRACTICE OF LATERAL-EFFECT POSITION-SENSITIVE SILICON PHOTODETECTOR

P.K. Buah-Bassuah[(a)], M. Melozzi[(b)], G. Longobardi

Istituto Nazionale di Ottica, Largo Enrico Fermi 6, 50125 Firenze
Italy

ABSTRACT

The theory outlining the principle and operational techniques of the lateral-effect position-sensitive silicon photodetector for enhancing the understanding of optical position sensing in different fields of application is discussed and re-appraised. A number of outstanding features of this detector in the areas of application are also treated and explained.

1. INTRODUCTION

The use of lateral-effect position-sensitive photodetector for optical position sensing in the last two decades is of much interest to researchers (1,2). This semiconductor device that converts received light signal (either temporal or spatial) to electrical signal using Lateral photoeffect, consists of a high resistant silicon wafer of intrinsic (I) material whose top surface is doped with boron to form a

p-layer and bottom surface with phosphorous to form n-layer to serve as an ohmic contact. With this structure, the device is designated as p-i-n photodetector. This opto-electronic sensor provides continuous dual-axis (x and y) position information of light spot transversing over its sensitive surface. Based on both theoretical and physical concepts in making this device, it is normally optimised or adapted with suitable optical components to serve the desired needs. However, its wide application is derived from its simplicity and accurate position sensing owing to its fast response speed, high position linearity and resolution (3-5). The optical position sensing could be monitored from transmitted or reflected light source on the object under investigation. Areas of application to be covered are in the fields of metrology, fluid dynamics, nuclear particle detection and colour vision. In these fields, the detector is used for angle measuring, nuclear particle sensing, vibration analysis, displacement and rotation monitoring. Moreover, other examples utilising this detector and collection optics include temperature monitoring of radiating surfaces and spectral response in colour vision. The features of this detector in obtaining high performance are also discussed.

2. THEORY

2.1 The lateral effect.

It is a well established fact that by the interaction of sufficiently energetic radiation normally incident on the active area of a semiconductor detector, there exists concentration of charge carriers at the interface of the p-n junction, generating a transverse potential difference across the sides of the same junction known as the transverse photovoltaic effect. The absorption of radiation at the point of uniformly irradiated junction results in the creation of electron-hole pairs at the interface of the junction. These electron-hole pairs get separated in opposite directions due to the electrostatic force at the

junction and thus modify the spatial distribution of the charges adjacent to the p and n region. The junction can therefore be compared to a current generator at steady-state condition under uniform illumination, whereby the generated photocurrent in external circuit functions from the incident radiation. If the illumination at the junction is however spatially non uniform (or when the region of interest of radiation or the active area of the photodiode is larger than the minority carrier diffusion length, one registers, in addition to the transverse photovoltage, a potential difference relative to the position of illumination and parallel to the same junction (6,7). In this mode of localised illumination, the process of electron-hole pairs, modifies the distribution of the minority carriers in only a small region of the opposite face of the p-n junction.

Such asymmetry that results, gives rise to an electric field component parallel to the junction as shown in Fig. 1a. The majority carriers on both sides of the junction can then move away parallel to the same junction from the zone of illumination. The p-n semiconducting material therefore presents a certain ohmic resistance from the number and mobility of majority charge carriers and a characteristic geometry of the region. As a consequence the produced lateral current is accompanied by the drop of potential in the transverse direction.

2.2 The fundamental equation

Deriving a functional relation between the point of illumination and the lateral current or the lateral photovoltage that results at the junction, it is necessary to consider the presence of the majority carriers at and away from the illumination zone in such a way that the generated current will vary in magnitude in regard to the recombination of minority carriers in a zone far from the illuminated region as shown in Fig. 1a. Before the separated carriers come up to the contact or the interface of the junction where recombination of carriers occurs,

obviously, there is reduction in the transverse photovoltage resulting in a deviation from equilibrium region. Consequently, the charges are transferred across the junction to re-establish equilibrium. Furthermore, the lateral field set up at the juncton enables the majority carriers of the separated charges to move from the point of illumination to the point of reinjection for rearrangement of carriers to establish charge neutrality.

In steady-state condition, the variation of lateral current in the chosen elemental volume $\Delta A W_n$ at Fig. 1a should be equal to the transverse current $J_T \Delta A$, where ΔA and W_n are the elemental area and the thickness of the undepleted n-type material as illustrated in Fig. 1a,b. The expression $J_T \Delta A$ must hold by considering also the contribution from the separation of the electron-hole pairs at the junction. If f(r) represents the total number of electron-hole pairs separated at the junction per unit time and per unit area at radius, r, then, f(r)=0 is at the outside of the illuminated zone. The expression of the transverse current J_T is given by

$$J_T \quad \Delta A = \left(J_S \left(e^{q\Phi(r)/KT} - 1 \right) - q f(r) \right) \Delta A \qquad (1)$$

where J_s = Saturation current

K = Boltzmann constant

T = Absolute temperature

q = Electric charge

$\Phi(r)$= Transverse potential difference.

By the law of conservation of charges, we have:

$$(\nabla \cdot J_L) \Delta A W_n = \left(J_S \left(e^{q\Phi(r)/KT} - 1 \right) - q f(r) \right) \Delta A \qquad (2)$$

where J_L is the lateral current density.

Simplifying eq.(2), it is assumed that p-region is at higher conductivity than n-region and p-region is considered as equi-potential. The lateral current density J_L in the n-region is then given by:

$$\nabla \Phi(r) / \varrho_n = - J_L \qquad (3)$$

where ϱ_n represents the resistivity of the n-region.

Substituting eq.(3) in eq.(2), one obtain

$$\nabla^2 \Phi(r) = \frac{\varrho_n}{W_n} J_S \left(e^{q\Phi(r)/KT} - 1 \right) + \frac{\varrho_n}{W_n} q f(r) \qquad (4)$$

where ϱ_n / W_n is the lateral sheet resistance of the diode substrate.

Eq.(4), which is differential, completely describes the lateral effect. However, this equation needs be linearized to obtain high linearity and resolution of the device. To achieve this objective, a small signal is considered that is, $\Phi(r) \ll KT$ and $\Phi(r) \ll -1$ for inverse polarisation. In the photovoltaic mode, eq:(4) becomes

$$\nabla^2 \Phi - \alpha^2 \Phi = - f_S \qquad (5)$$

where $\alpha = \left(\frac{\varrho_n}{W_n} \frac{J_S}{K} \frac{q}{T} \right)^{1/2}$ is the Lucosky fall-off parameter and

$$f_S = \varrho_n / W_n \, q f(r)$$

In the photoconductive mode, we have the exponential term in eq.(4) being negligible under fully reverse biased condition. We have

$$\nabla^2 \Phi = - (f_S + f_d) \qquad (6)$$

with $f_d = \varrho_n / W_n \, J_S$

According to /9/, eq.(6) can be considered in a particular case as in eq.(4) when $\alpha = 0$. When the luminous signal is a function of time, eq.(5) then becomes /7/

$$\nabla^2 \Phi - \alpha^2 \Phi - \beta \frac{\partial \Phi}{\partial t} = - f_S \qquad (7)$$

where $\beta = c \varrho_n / W_n$ is the time constant per unit area.

The validity of eq;(6) and eq.(7) can be extended to any value of polarisation signal which indicates that α and β have more complex expression and are functions of the polarization voltage (10,11).

2.3 The steady-state condition.

In order to obtain practically the lateral potential difference or alternatively the lateral current, it is necessary to introduce some thin layer at the bottom surface of the n-substrate of the silicon wafer. The introduction of this contact determines the steady-state condition of the equation previously derived and defined. Analytic solution of eq.(7), would appear possible only for infinite terminating impedances at the lateral contacts which imply that the field strength component $\partial\Phi/\partial x$ normal to the boundary or the contact must be zero ($\frac{\partial \Phi}{\partial x} = 0$) or there must be a zero impedence ($\Phi = 0$) at the same lateral contacts along the junction side.

Supposing that the luminous signal is mathematically represented as

$$F(x,y,t) = F_O \, \delta(x - x_O) \, \delta(y - y_O) \qquad (8)$$

for $t > 0$ (step signal), where $F_O = I_O \varrho_n / W_n$ and the generated photocurrent, Io, $Io = PR_\lambda$; where P is the monochromatic incident power and R_λ the detector responsivity at that wavelength. Eq.(7) can be

written as Fourier series given by:

$$\Phi(x,y,t) = F_0 \sum_{m=-\infty}^{+\infty} \sum_{n=-\infty}^{+\infty} \sin(m\pi x/\ell + \vartheta)\ \sin(m\pi x_0/\ell + \vartheta)\cdot$$

$$\sin(n\pi y/\ell + \psi)\ \sin(n\pi y_0/\ell + \psi)\cdot$$

$$\left(\left(1 - \exp\left(\alpha^2 t^2 + (m^2 + n^2)\pi^2 t/\beta \ell^2 \right) \right) \right) \qquad (9)$$

where ℓ is the contact length and the value of the phases ψ and φ is determined by introducing the steady-state condition.

When $\varphi = \psi = \pi/2$, it corresponds to a particular case of infinite impedance, whilst $\varphi = \psi = 0$ implies the condition of zero impedance $\Phi(0) = 0$.

In order to obtain a device of high linear response, various types of diode configuration based on the steady-state conditions derived from Eq.(7) are then considered.

2.3.1 Wallmark Diode

Figure 2 shows the configuration of applied infinite impandence at the four sides of the photodiode, that is, ($\psi = \psi = \pi/2$). In a steady-state condition ($t = \infty$), Eq.(7) indicated that the potential at the midlateral point contact $(0, 1/2\ell)$ is

$$\Phi(o, \ell/2) = F_0 \sum_{n=-\infty}^{+\infty} \cos(2n\pi y_0/\ell) \cosh a_n (1 - x_0/\ell) \,/\, a_n \sinh(a_n) \qquad (10)$$

with $a_n = (\alpha^2 \ell^2 + 4n^2\pi^2)^{1/2}$ and as there is no external current it implies $\alpha = 0$. For other points of the contact, the value can be calculated, neglecting the axes of reference and substituting (Xo,Yo) by $(\ell - Xo, \ell - Yo)$. It is important to note that the potential at point $(0, \ell/2)$ is a function of both coordinates of the illuminated position.

Therefore, on the same axes, values of $\Phi(0, \ell/2)$ are still functions of Yo. Besides this response, this type of position sensing detector does not describe linearity with respect to the point of illumination. It can be demonstrated, however, that the logarithmic ratio of the output signals per axis is linearly related to the light spot position along that axis for the central diode area as shown in Fig. 3. Since α is a function sensitive to temperature, the utilisation of this configuration just discussed for practical application is very critical and unsuitable in terms of linear response.

2.3.2 Duolateral sensor

Figure 4 shows electrodes on two sides of the n-region (at x=0, $x = \ell$) of the same contact . In this mode when $\varphi = 0$ and $\psi = \pi/2$, the steady-state solution at $t = \infty$ of Eq.(7) becomes

$$\Phi(x, y, \infty) = F_0 \sum_{m=-\infty}^{+\infty} \sum_{n=-\infty}^{+\infty} \Big(\sin(m\pi x/\ell) \sin(m\pi x_0/\ell) \cdot$$

$$\cos(n\pi y/\ell) \cos(n\pi y_0/\ell) \Big) \Big/ (\alpha^2 \ell^2 + (m^2 + n^2)\pi^2) \cdot \qquad (11)$$

$$\left(1 - \exp\left(-\left(\alpha^2 \ell^2 + (m^2 + n^2)\pi^2 \right) t/\beta \ell^2 \right) \right)$$

The current across the contact (x=0) is given by

$$I(o, y, \infty) = \frac{W_n}{\varrho_n} \int_0^{\ell} \left. \frac{\partial \Phi}{\partial x} \right|_{x=0} dy = I_0 \sinh\left(\alpha(\ell - x_0/\ell) \right) / \sinh(\alpha \ell) \qquad (12)$$

The difference between this configuration and that of Wallmark is: the output current signal is no more a function of Yo coordinate of the position of illumination. Lateral effect in the duolateral case is caused by current distribution at lateral contacts under fully reverse biased mode whilst that of Wallmark depend on diode surface recombination of carriers. The precedent expression is a function of α-parameter and the solution of interest is the one which the α-parameter holds at zero implying that the diode is inversely

polarised at fully reverse biased mode. Upon this reason, Eq. (12) becomes

$$\lim_{a \to 0} \quad I(0, y, \infty) = I_O(1 - x_O/\ell) \qquad (13)$$

We can conclude that the present system in this condition, as expressed in Eq.(13); gives a high linear response with respect to the position of illumination as shown in Figure 5a. The output signal can be made independent of the intensity of radiation Io.

RETRIEVAL OF POSITION MEASUREMENTS FROM LATERAL EFFECT

Referring to Figure 5b(i), (ii) and using Eq.(13) at each axis or electrode of the sensor, position measurements are obtained from their output signals' as follows:

$$I_1 = I_O(\ell/2 - x_O)/\ell) \qquad (13a)$$

$$I_2 = I_O([\ell/2 + x_O]/\ell) \qquad (13b)$$

similarly at the other axis or electrodes we have

$$I_3 = I_O([\ell/2 - y_O]/\ell) \qquad (13c)$$

$$I_4 = I_O([\ell/2 + y_O]/\ell) \qquad (13d)$$

We substract Eqs. (13a) from (13b) to obtain surface current proportional to the product of spot position and intensity

$$I_2 - I_1 = (x_O/\ell)\, I_O \qquad (13e)$$

We add Eqs. (13a) to (13b) to get a relation of the surface currents being proportional to spot position

$$I_2 + I_1 = I_O \qquad (13f)$$

In order to obtain the position of output signal independent of intensity of radiation, Eq. (14) is divided by Eq.(15) to arrive at an expression thus:

$$\text{x position:} \quad \frac{I_2 - I_1}{I_2 + I_1} = x/\ell \qquad (13g)$$

similar argument could be followed to obtain expression for y position as:

$$\text{y position:} \quad \frac{I_4 - I_3}{I_4 + I_3} = y/\ell \qquad (13h))$$

x and y are the coordinate positions of the light spot.
Measuring the coordinates at point of illumination, one can apply pairs of electrodes on both faces of the junction as shown in Figure 5c. However, for a given value of interelectrode distance or contact length ℓ, the aspect ratio ℓ/w_n must be above certain value, say 10, to maintain lateral photoeffect.

2.3.3 TETRALATERAL SENSOR

In this configuration, the sensor has four electrodes on upper surface of the diode with lateral contacts applied along all sides with negligibly small spacing between adjacent contacts as shown in Figure 6. With this configuration, however, $\psi = \varphi = 0$, and the expression of the current $I_{x=o}$ obtained in analogous way of the precedent case is

given by

$$I_x(0,t) = 2I\pi I_O \sum_{n=-\infty}^{+\infty} \sin\left(\frac{(2n-1)\pi y_O/t}{2n-1}\right) \cdot$$

$$\left(\frac{\sinh(a_n(1-x_O/t))}{\sinh(a_n)} - \sum_{m=-\infty}^{+\infty} \frac{m\pi \sin(m\pi x_O/t)}{(a_n^2+m^2\pi^2)}\right) \cdot \qquad (14)$$

$$\exp\left(-(a_n^2+m^2\pi^2)/t/\beta t^2\right)\Big)$$

where $a_n = \left(\alpha^2 t^2 + (2n-1)^2\pi^2\right)$

Once more, as in the case of the Wallmark diode, the output signal as seen in Eq. (14) and Figure 7a is also a function of Yo coordinate. Therefore, for the tetralateral diode, the logarithmic ratio of the output signals present is somewhat a linear behavior. It is demonstrated, then, that the linearity of the system can be furthermore improved if the lateral contact is slightly curved, that is, the pin-cushion type. Figure 7b illustrates the effect of the linearity of this device.

2.4 TEMPORAL RESPONSE

The temporal behavior of the output current for bilateral configuration and pulse input signal has response as shown in Figure 8 as a function of $t/\beta t^2$, and at equal value of x_O/t. This photodiode is supposed to be inversely polarised. In this condition, one has the depletion layer widened with high bias voltage so that there would be a reduction in capacitance. This effect is shown on Figure 9 for the two configurations. If it is possible to neglect the transit time of the charges (which naturally increases with the depletion layer), the inversely polarised diode presents a shorter response time than an unpolarised diode. The response time is a function of position or the

point of illumination and increases also with the distance of the contact /12/. The necessary and sufficient condition to obtain a meaningful response is after a time of $t/\beta t^2 = t/RC t^2 \gg 1/2$. It can therefore be deduced thus, the frequency response bandwidth /3/ that dictates on the resolution of the detection is given by:

$$f_c = (\pi/2)/(R\,C\,t^2) \qquad (15)$$

The typical response time is of the order of 2.5-50 μs for arriving at a time of about 70 μs /9/. Finally, the impulsive response of a duolateral was compared with tetralateral configuration and /9/ found that the lateral configuration was faster. Figure 10 shows the spectral response sensitivity for the two types of diodes.

2.5 TEMPERATURE DEPENDENCY

The temperature dependency on the system essentially increases with α-parameter since the diode inverse saturation current density is sensitive to temperature variations. In this mode, however, when $\alpha = 0$, the temperature dependency can be considered negligible apart from noise effects as experimentally verified at low temperatures /13/. Therefore, under zero impedance mode operating between 400 to 900 nm, the position sensitivity is not affected by temperature characteristics.

2.6 SPATIAL RESOLUTION

To calculate the minimum resolvable spatial variation, for example in the x-direction, it is necessary to compare the signal current variation ΔI_x produced by incremental change in position Δx and in turn compare with the noise of the system. The detector noise current I_d term is given by:

$$I_d = \left(\frac{4KT}{R_S}\right)^{1/2} \qquad (16)$$

where R_s is the resistance between back contacts.

This is the principal noise source which determines the condition of linearity of the apparatus and require also small impedance R_s for the lateral contact. Together with Johnson noise, we considered the contribution of noise associated with the nature of incoming photons that results as carriers. This is the short noise of the dark and signal currents given by:

$$I_q = (2 q I_o)^{1/2} \qquad (17a)$$

where Io is the intensity of the current and E is the amplifier input-noise voltage.

The effective input-noise current I_v is $I_v = E / R_s$. The total noise current, I_R, supposed to be white, is then given by:

$$I_R = \left(\frac{4KT}{R_s} + \frac{E^2}{R_s^2} + 2 I_o q \right)^{1/2} (\Delta \nu)^{1/2} \qquad (17b)$$

From the other part of variation ΔI_x is associated with the displacement Δx given by:

$$\Delta I_x = \frac{I_o}{t} \Delta x \qquad (17c)$$

The signal-to-noise ratio is equal to unity which has minimum resolvable displacement Δx_m expressed as

$$\Delta x_m = t \frac{\left(\frac{4KT}{R_s} + 2 I_o q + \frac{E^2}{R_s^2} \right)^{1/2} (\Delta \nu)^{1/2}}{I_o} \qquad (17d)$$

Obtaining a value of order-of-magnitude, Δx_m with figures of (S1544 HAMAMATSU Detector) of length 6 mm with a back-contact resistance R_s of 10 kiloohm being illuminated with 2 μW light spot at detector's responsivity of 0.6 A/W at a wavelength of 900 nm in a circuit with an amplifier input-noise voltage of 10 μV at a frequency band width of 10KHz, it was evaluated as 0.37 μm which is the minimum resolvable displacement.

3. FABRICATION OF THE DETECTOR

The resistive layer of detector can be made by either Diffusion or Ion implantation to yield high linearity and high performance (14;15). Both methods use the P-I-N Structure configuration and attain the same form as shown in Figure 12.

3.1 Diffusion

Boron (p-type) is doped by diffusion on the front surface of silicon wafer and phosphorous on the back surface at temperatures between 850°C and 1150°C. The device is annealed to ensure ruggedness whilst the contacted layers determine dynamic response and reduce noise. An active area is grown with SiO_2 on the diode surface to serve as anode and then contacted with aluminium wire. Metalisation is done with aluminium and then gold contact on the surface of n-layer using vacuum evaporation. The aluminium layer on the whole surface acts as an optical reflector to improve sensitivity at longer wavelengths where the incident light normally penetrate the silicon and gold film ensures stable and low resistance contact. This method is quite simple and ensures high resolution but it is not effective for large active areas more than 1·5 cm^2.

3.2 Ion Implantation

Using an isotope separator, beam of ions of P^{31} up to 30 μA and B^{11}

up to 10 μA are implanted on the back and front of silicon wafer respectively placed in a drum in a vacuum chamber. The ions lie within a shallow layer (0.1 to 0.8 μm) horizontally on the silicon surface to yield homogeneous sheet resistivity of about 20 times higher than the corresponding doped diffused layer of 2 to 4 μm thickness. The substrate is annealed for uniformity and the wafer contacted with gold strips for good electrical connection. The active area is coated with photoresist and etched with silicon to remove the unprotected parts of the implanted layers. Aluminium metalisation at the bottom part of n-layer is done to serve as an optical reflector.

This method has an advantage over the former because it avoids precipitation and impurity of concentration in the substrate. This method of ion implantation can make devices of high active area owing to the high resistive sheet and the choice of junction capacitance. However, the device from this method is expensive. Ion implantation detector has found more effective use for particle counting in some areas of Nuclear Physics than the diffusion type.

The Table 1 below shows basic parameters to consider when fabricating a typical duo-lateral type diode substrate. They include the sheet resistivity, terminating impedances, reverse voltage and junction capacitance needed to determine the lateral-effect contacts in order to improve the linearity of the device.

TABLE 1

Parameters	Method of Fabrication	
	Hamamatsu 1300	Selcom AB C° 2L24
	Planar Diffused type	Ion implantation type
Active area	(13 x 13) mm^2	(24 x 24) mm^2
Intensity sensitivity (Responsivity)	0.55 A/W at 900 mm	0.6 A/W at 950 mm
Position Resolution	6 μm	0.1 μm
Position Linear error	0.5%	0.5%
Resistive Sheet R_s	10kΩ /cm^2	10kΩ /cm^2
Leakage Current	1 μA	1 μA
Junction Capacitane C	200 pF/cm^2	45 pF/cm^2
Bias Voltage V_R	20 V	50V (maximum)
Rise time	8 μs	0.1 μs
Noise in Differential Output current	1 nA	1 nA
Operating temperature	-10°C to 60°C	-10°C to 60°C

The fabricated diode substrate in Figure 12 is insulated with an epoxy, hermitically sealed, mechanically masked in a housing and finally mounted in aluminium header before it is used.

4.

4.1 The Read out Electronics

The theory used to retrieve position measurement is practically related here to the read out of the output signals from an electronic circuitry based on differencing, summing, and division using a network of analog amplifiers and dividers as shown in Figure 13. The first amplifier stage is operated in transimpedance mode which boost the photodetector current by converting it into voltage. The output of each of these amplifiers is fed to a sum and difference amplifiers such that the difference signal is proportional to spots intensity and that of the sum signal to only intensity. The divider network ratio out the two signals to obtain required position. The final signal is fed into a buffer amplifier which drives the digital display into analog position outputs. Relating therefore to Eq.(13g) and Eq.(13h), position measurements are practically obtained as:

$$\text{x position} = \frac{K(A - C)}{A + C} \qquad (18)$$

$$\text{y position} = \frac{K(B - D)}{B + D} \qquad (19)$$

where K is the gain factor of the amplifiers and A,B,C and D are the electrodes connected to respective amplifiers.

OPERATIONAL EQUIVALENT CIRCUIT

Applying the above concepts and principles earlier on outlined, one can make an equivalent circuit of the device as shown in Figure 14. The generated photocurrent I_s by the light on the active area on the substrate is divided by the multiple ohimic contacts which are the resistive sheets R_{s1}, R_{s2} at the front and back n-layer where the electrodes x and y are connected in pairs. The output currents displaced along the four electrodes have the x-position proportional to (I_2-I_1)

and y-axis to (I_4-I_3). We ratio out the output signal so as not to be affected by intensity. These quantities are divided out by the sum of the photocurrents along the corresponding axes to yield the expressions shown at Eq.(18) and Eq.(19).

4.2 Experimental configuration

The fundamental aspects of this detector and its read out electronics were treated to enable us to outline and highlight on the general applications of this device in some fields of study. the detector, placed in a configuration shown in Figure 15, converts the received light source with the aid of optical components through or on the media (either transmittive or reflective) under test, into an electric signal which is then viewed on the oscilloscope. The read out electronics of the detector is interfaced with an analog digital converter and a microcomputer. In this way, the electrical signal can easily be processed and analysed.

5. SOME FIELDS OF APPLICATION

5.1 Metrology

The position sensitive detector is incorporated in an opto-electronic system to sense simultaneously vibration and displacement of an object /16/. The set up of the system is shown in Figures 16 and 17. The split beams are targeted at an angle φ onto a mirror fixed on the surface under investigation and then become deflected onto two photodetectors at a distance L cm away in order to distinguish the longitudinal translation from the angolar rotation of the body. The x and y output signals of the detector are connected to electronic parts and an Olivetti (M24) by 12 bit 4 input analog digital converter for both data acquisition and processing. The displaced beam d from the surface translates through a distance D and rotates through an angle α given by an expression,

$$d = 2D \sin\varphi + \left(\frac{2\cos\varphi}{\cos\varphi} + L\right) \tan 2\alpha \qquad (20)$$

when $\varphi = 0$ and $L >> D$

$$d_1 = L \tan 2\alpha \qquad (21)$$

when $\varphi \neq 0$ and $L >> D$

$$d_2 = 2D \sin\varphi + L \tan 2\alpha \qquad (22)$$

The variation of the position of the beams is deflected by the different photocurrents displaced along the four electrodes of the detector. The currents I_1 and I_2 from the two photocurrents PSD1, PSD2, are proportional to Eq.(21) and Eq. (22). α is directly calculated from I_1, and that of D evaluated from the difference between I_1 and I_2.

Measuring translation and rotation

A small mirror is attached to the membrane of the small loudspeaker which is mounted on a large loudspeaker. The large loudspeaker translates linearly by a low frequency signal 1Hz since its edges are not fixed and the small loudspeaker rotates about its fixed edge driven by high frequency signal of 3Hz when their coils are excited. This arrrangement was to separate the rotational and translational motions. Figure 18a,b shows the joint effect of the two motions and the other only that of the rotational motion respectively. BY evaluating the relative frequency spectrum of Figure 18a,b, a lower frequency contributed by the translation motion from the large loudspeaker is obtained as shown at Figure 19. This frequency was calulated from the total displacements on the PSD and resultant evaluated from the data acquired on the x and y axes.

Measuring vibration of motor shaft

A laser beam is incident at the mirror fixed to a rotating shaft of an electric motor. The deflected laser beam is received by the position sensing photodetetor. If the shaft is not rotating perpendicular to its axis or the mirror is not fixed in its plane, the rotation will describe a cone, that is, a circle on the surface of the detector. To avoid this, a reference circle representing the shaft rotating at low frequency is taken as the reference circle during vibration and any deviation from it is taken as noisy trajectory. In order to extract vibration at Figure 20 the reference line of oscillation was scaled out and frequency spectra for different rotational velocities obtained as shown in Figure 21. The sample time for data acquisition and analyses was 30 μs with frequency higher than 3KHz. Limitation of the system was above the range of 3KHz to 10KHz and was due to the drift of detector and the analog electronics. With L=40 cm, α=30°, rotational and translational sensitivities of 0.005 deg/Volt and 100 μm/V were respectively measured /16/. Typical detector UDT-SC10D which had resolution of 1-2 μm, an active area of 103 mm^2 and a field of view of 140° was used. Its response was 0.4 A/μW at 900nm with rise time of 100 ns. The uniformity of this detector was $\pm$ 2% with position sensitivity of 0.5 A/W/cm.

5.2 Fluid Dynamics

The second application is in the field of fluid dynamics for the study of temperature regime in fluids in transparent cell /17/. With the aid of optics, electronics and scanning mechanism, this same lateral-effect photodiode measures deflection angles at different position of the medium under test by first calibrating the lens and the cell. The position information is retrieved from the disuniformity field in the transparent liquid medium caused by the thermal gradient. The principle of this system is shown at Figure 22a. A laser beam at an

angle γ with the optic axis at point $Q(q,o)$ reaches s at coordinates (s,do) and the same point at coordinates (s,dl) when it become deflected at $t(t,h)$. The angle of deflection is derived from the difference in lateral displacement of the spot given by:

$$d_1 - d_0 = \frac{\left(s - (s-f)\tan\vartheta\right)\left(1-\tan^2\gamma\right)\tan\vartheta}{1 + \tan\vartheta\,\tan\gamma} \qquad (23)$$

where f is the focal lenght of L

when s=f and γ=0, d = 0 (24)

$$d_1 = f \tan\vartheta$$

Practically, as shown schematically at Figure 22b, two mirror galvanometers M_1, M_2 serving as scanners for x and z axes are placed at the focus of lens L_2 which is confocal with lens L_1 and of the same focal length to avoid divergence of the beam in the testing region. The sweeping beams exit parallel through the test region and are collected by lens L_3 at whose focal length this photodetector is placed. The point of traverse at x,z by bidimensional sweep is set for total number of horizontal lines N_2 from 1 to 256 given by an expression:

$$x = \frac{L_x}{T}\,t \qquad 0 < t < T$$

$$z = \frac{L_z}{N_z}\,n \qquad 1 < n < N \qquad (25)$$

where T is the period of incident wave that drives the galvanometer, and L_x, L_z are lengths of x and z sweeps with n a number of particula line. t is the time.

The output of the detector is connected to amplifiers for normalisation

with respect to intensity and fed into a 12 bit analog digital converters interfaced with microcomputer to memorise data. The output voltages are proportional to the coordinate (x',z') of the weighted average of the light distribution on the detector surface given by:

$$V = A\,X'$$

$$V = A\,Z' \qquad (26)$$

where A=3.9 V/mm and is the gain factor of the detector and its electronics.

From Eq. (24) and Eq.(26), the output voltages become:

$$V_x(X,Z) = A\,f_3\,\vartheta(x,z)$$

$$V_z(X,Z) = A\,f_3\,\vartheta(x,z) \qquad (27)$$

For f_3=30 cm, maximum angle of $\vartheta(x,z)$ was obtained as 0.01 rad. To account for and avoid errors, initial sweeps of scanning pulses F_h, S_h at ϑ = 0 yielding voltages Vox, Voz were stored in the computer and substracted from voltages Vx, Vz obtained from the sweeps through the testing region onto the detector for each angle ϑ_x, ϑ_z to obtain Vx(x,z)-Vox(x,z) and $V_z(x,z) - V_{oz}(x,z)$ respectively.

Calibration

The system was calibrated using a plano convex lens placed at the testing region and its surface scanned to obtain the focal length of the lens (f) from the detected beam. Working within paraxial ray region given by $y = (X^2+Z^2)/2f(n-1)$. The deflecting angles of the laser beam expressed as:

$$\vartheta(x,z) = \frac{x}{f}$$

$$\vartheta(x,z) = \frac{z}{f} \qquad (28)$$

were used addition to Eqs.(24),(26),(27) to arrive at general equation of

$$V_x - V_{ox} = A\ L_x f_3\ t/T\ f$$

$$V_z - V_{oz} = A\ L_z\ f_3 n / N_2 f \qquad (29)$$

from which the focal length of the lens f was found with the aid of the slope from graph at Figure 23a.

The sensitivity of the lateral-effect photodetector is shown by the surface profile at Figure 23b. Measurements made on this lens at different positions gave an error of 1%.

The cell was calibrated without fluid. An empty plexiglass cell was heated from above with spatially periodic source with its lower part kept at constant temperature. The previous procedure was repeated with this cell when it was heated and without heating source to obtain voltage $V_x - V_{ox}$ and $V_z - V_{oz}$. The deflected beams resulting from the thermal gradients were given by

$$\vartheta_x(x,z) = L_y \frac{\partial n}{\partial T} \frac{\partial T(x,z)}{\partial x}$$

$$\vartheta_z(x,z) = L_z \frac{\partial n}{\partial T} \frac{\partial T(x,z)}{\partial z} \qquad (30)$$

where $\frac{\partial n}{\partial T}$ is the thermal coefficient of the refractive index of plexiglass and L is the thickness of the cell.

The temperature gradient was averaged along y in an array of 16 rows with 64 points each. Integrating the two derivatives $\partial T/\partial x$, $\partial T/\partial z$

$$T(x,z) = \int_o^x \frac{\partial T(\tau, z)}{\partial x} d\tau + \int_o^z \frac{\partial T(o,a)}{\partial z} da \qquad (31)$$

the temperature field of the empty cell was reconstructed as shown in Figure 24.

STUDY OF TEMPERATURE REGIME OF HEATED OIL

The cell was filled with silicon oil (47V100) and heated from below with its top maintained at constant temperature. The spatial periodic heating source was switched on and then later switched off. The image was recorded every two minutes from when the heat was switched on up to 29 minutes. At the first two minutes, conduction was realised from the cell but at later time up to 29 minutes convective regimes were seen. The sensed image by the detector gave position information from the relation of the temperature gradient in horizontal and vertical shifts as:

$$dx = f_3 \frac{\partial n}{\partial T} \frac{\partial T}{\partial x} L_y$$

$$dz = f_3 \frac{\partial n}{\partial T} \frac{\partial T}{\partial z} L_y$$

at all positions of the (x,z) plane. The temperature field was recovered by numerical integration of the two recorded gradients as shown in Figure 25.

5.3 COLOUR VISION

In radiometers, the silicon photodetector is incorporated to measure radiance and luminance with the aid of monochromators or filters /18/. The position sensitive detector is the primary converter of the measured optical radiation into electric signals that are later amplified and processed. In photometry, a detector must have sensitivity over the range of 380 to 780 nm, which is defined by the CIE to be the visible spectrum. To measure the broad band incident radiation, the photodetector must conform to a spectral response that matches the CIE

V_λ curve. To adapt this detector to have such response, an external filter which consist of layers of subtractive coloured glass is combined with the detector to flatten the spectral response of the material to the required working range of 450-950 nm of the detector, as shown in Figure 26a. The optical radiation, in radiance, is measured with addition of a lens of well defined field of view which targets the deflected light from the material or surface whose colour is being monitored. The collected image of the lens is filtered and then focused onto the detector. These detectors produce a photocurrent proportional to the amount of the incident light.. The amplifier in a transimpedance stage amplify the input current and output into a voltage. The responsivity of the detector is given by R_λ =current/optical unit and the tranimpedance of the amplifier is expressed as T=Voltage/current. The resulting voltage $V=R_\lambda$ xT=Volts/lumens or Volts/Radiance.

By interfacing the detector with analog digital converter and microcomputer, the data acquisition and processing could be easily done. Figure 26b shows the block diagram of the general configuration.

5.4 NUCLEAR PARTICLE DETECTION

A measurement of position resolution and linearity for a one dimension detector having a sensitive area of 4x32 mm as shown in Figure 27a is consistent with two-dimension square detector of $(10x10)mm^2$ /13-15/. Am^{241} alpha particles were incident through a mask containing 15 slits, each 1.00 mm wide separated 2.00 mm on centres onto the one dimension detector. One of the slits near one end of the detector was covered with tape to provide a convenient identification of the detector orientation during testing. The results showed the uniformity and stability with ion implantation layer instead of the diffusion type of detector. The straight line was obtained from a least square fit with maximum deviation less than 1%. The position resolutions obtained on $(10x10)\ mm^2$ at room temperature was 0.3 - 0.5 mm F.W.H.M. in both x and

y directions and its distribution of x and y ratio pulses due to admitted alpha's of masked detector as shown at Figure 27b.

In this case cross "x"-shaped mask slits each 13x0.5 mm was used.

To test for the response of the detector, a beam of oxygen ions in a mixture of charge states was created by passing the accelerated beam through a thin carbon foil. Each selected ion by an appropriate setting of the switching magnet was passed through analysing magnet into the detector without altering the field in the analyser yielding a spectrum shown at Figure 28. Position information was retrieved from the group of ions in relation to their different masses and energies. The relative population of the charge state groups were simulatenously and instantly measured. Since energy of these ions are discrete, there are absence of counting between the peaks. The low energy tails on the 6^+, 7^+, 8^+ were caused by slit scattering in the collimating system used. The maximum deviation from linearity was 3 channels or less than 1% of the detector length.

In another application, a beam of 12 MeV protons were directed onto and scattered from a 200 $\mu g/cm^2$ target of Yb^{171}. Elastically scattered protons and inelastically scattered protons populating the energy levels of 66 and 76 keV were observed in the detector. In this measurement, the detector was installed at the focal plane of the broad range charges particle spectrometer. The measured position resolution spectrum is shown at Figure 29.

6 CONCLUSION

The theory and practice of lateral photoeffect on silicon position-sensitive detector has been analysed. Of course, p-i-n lateral effect photodetectors are not the only ones for position sensing applications.

More sophisticated solutions make use of linear or matrix arrays of photodetectors, where the light spot intensity can be mapped and its

centroid searched with suitable alogarithms /19/. Compared to the discrete element detectors such as charge coupled device (CCD), /20/, the position-sensitive lateral-effect photodetector features high resolution, fast response speed, and simple operating circuits. The advantages of the single lateral-effect silicon position-sensitive photodetector is instead in its simplicity, high sensitivity, realiability and high linearity, still allowing for accurate position sensing, even exceeding the Rayleigh criterion for optical system resolution.

ACKNOWLEDGEMENT

The authors are much indebted to Prof. F.T. Arecchi for his encouragement and very useful suggestions.
One of the authors, P.K..B-B. was supported by International Centre for Theoretical Physics, ICTP, Trieste, Italy, Laboratory training programme at Istituto Nazionale di Ottica, Firenze, Italy.

REFERENCE.

a) On leave from Department of Physics, University of Cape Coast, Cape Coast, Ghana, on ICTP, Trieste, Italian Labs training Programme.

b) Officine Galileo, Campi Bisenzio, Firenze, Italy.

1. B.O. Kelly, "Lateral-effect photodiodes", Laser Focus pp.38-40, March,1976.

2. B. Light, "Optical Position sensing using silicon photodetectors", Laser Focus, Vol.V, N°4,pp.75-79, April, 1986.

3. G. Lucosky and R.B. Emmons, "Lateral Effects in High-speed Photodiodes", IEEE Trans-Electron Devices, ED-12,5,(1965).

4. G.P. Petterson and L.E. Lindholm, "Position sensitive light detectors with high linearity", IEEE Journal of Solid State Circuits, Vol. SC-13, N°3, pp. 392-399, June, 1978.

5. V. Radeka, "Signal noise and resolution in position-sensitive detectors", IEEE Trans. Nucl. Sci. Vol.21, pp.51-64, Feb. 1974.

6. J.T. Wallmark, "A new semiconductor photocell using lateral photoeffect", Proc. IRE, Vol.45, pp.474-483. April 1957.

7. G. Lucosky, "Photoeffects in non-uniformly irradiated p-n junctions",J. Appl. Phys. Vol.31, pp.1088-1095, June, 1960.

8. R.B. Emmons, "The lateral photoeffect", solid state Electron. Vol.10,pp.505-506, May, 1976.

9. H.J. Woltring, "Single and Dual axis lateral photodetectors of rectangular shape", IEEE Trans. Electron Devices, Vol.ED-22 pp.581-586, Aug. 1975.

10. D.A. Allen, "An analysis of the radiation tracking transducer", IRE Trans Electron Devices, Vol.ED-9, pp.411-416, Sept.1962.

11. W.P. Connors, "Lateral photodetector operating in the fully reverse biased mode", IEEE Trans. Electron Devices, vol.ED-18, pp.591-596, Aug.1971.

12. C.A. Klein and R.W. Bierig, "Pulse-response characteristics of position-sensitive photodetectors", IEEE Trans. Electron Devices", Vol. ED-21 pp.531-537, Aug. 1974.

13. E. Elad and R. Sareen, "Low temperature characteristics of ion implanted silicon position sensitive detectors", IEEE Trans. Nucl. Sci. Vol.21, pp.75-84, Feb.1974.

14. R.B. Owen and M.L. Awcock, "One - and two - dimensional position sensing semiconductor detectors", IEEE Trans. Nucl. Sci., Vol.15, pp.290-303, June, 1968.

15. E. Laegsgaard, F.W. Martin, and W.M. Gibson, "Position-sensitive semiconductor particle detectors fabricated by ion implantation", IEEE Trans. Nucl. Sci. Vol. NS -15, pp.239-245, June, 1968.

16. F. Francini, M. Macchiarulo, B. Tiribilli, P.K. Buah-Bassuah, "Opto-electronic system for displacement and vibration measurements", Rev. Sci. Instr. Vol.58, n°9, pp.1678-1681, Sept.1987.

17. S. Ciliberto, F. Francini, and F. Simonelli, "Real-Time measurements of optical disuniformity fields", Opt. Comm. Vol.54, N°5, pp. 251-256, July, 1985.

18. Ian Edwards, " Radiometry/Photometry: A modular approach", Photonics Spectra, Vol.21, Issue 5, pp. 57-62, May, 1987.

19. W.J. Price, Nuclear Radiation Detection, - Chap 8 "Semiconductor radiation detectors", McGraw-Hill Bk. C° pp. 215-266 New York, 1964.

20. C.J.S. Damerall, F.J.M. Farley, A.R. Gillman and F.J. Wickens: "Charged-Coupled devices for particle detection with high spatial resolution", Nucl. Instr. Methods, 155,33 (1981).

FIGURE CAPTIONS

Fig.1. a) The charge and potential distribution of lateral photoeffect.

b) The behaviour of the transverse potential difference $\Delta\ \Phi(r)$ and lateral potential difference (ΔV_L) of lateral photoeffect.

Fig.2 Bottom view of dual-axis square Wallmark diode with floating junction.

Fig.3 Dual-axis Wallmark diode. Loci for constant values of log output potential ratio per axis log (X+/X-) or log (Y+/Y-), for equidistant fractions of log ratio. Constant corresponding to the 90% off-center axial point.

Fig.4 Bottom view of single-axis duo-lateral detector.

Fig.5 a) Output signals from a double-sided duolateral detector showing the high position linearity.
b) Sectional views of duo-lateral detector (square type) showing retrieval of position information.
(i) sectional fron view (ii) Bottom view.
c) Dual-axis duo-lateral diode with two electrodes each on upper and lower surfaces of the diode substrate.

Fig.6. Dual-axis tetralateral sensor.

Fig.7. a) Dual-axis tetralateral diode. Loci for constant values of the output current ratio per axis log (X+/X-) or log (Y+/Y-), for equidistant fractions of the log ratio. Constant corresponding to the 90% off-center axial point.
b) Linear response of the pincushion dual-axis tetralateral detector.

Fig.8. Short circuit current response to step input of radiation with distance from contact as a parameter and α=0.

Fig.9. A plot of Capacitance vrs. Reverse voltage for the duolateral and tetralateral sensors.

Fig.10 Normalised spectral response of Duolateral and tetralateral sensors.

Fig.11 Temperature characteristics of spectral response of (i) Duolateral (ii) Tetralateral sensors.

Fig.12.Cross sectional view of lateral-effect position sensitive photodetector.

Fig.13.The electronic Readout circuit.

Fig.14.Equivalent circuit of Duo-lateral sensor.

Fig.15.Configuration for general application.

Fig.16.Block diagram of the optical device.

Fig.17.The Optical probe.

Fig.18.a) The displacement of the Beam B.2 on PSD2 due to rotational and translational effect of the surface.
b) The displacement of the beam B on PSD1 due to only rotational effect.

Fig.19.a) The relative frequency spectrum of fig.18 (a).
b) The relative frequency spectrum of fig 18 (b).

Fig.20.The vibration of the rotating shaft of electric motor. The external and internal curves are respectively relative to velocities of 50 rev/s. and 150 rev/S.

Fig.21.The relative frequency spectrum of the signal at Fig.20.

Fig.22.a) The optical system illustrating the principle of the device.
b) Experimental configuration: M1 , M2 moving mirrors, G1 ,G2 , galvanometers, L1 ,L2 ,L3 lenses, Position Sensitive detector PSD, Detector Electronics DE, Analog/Digital Converter ADC, microcomputer, Scanner Driver SD.

Fig.23.a) deflection angles $\vartheta_x(0,z)$ (Triangle), $\vartheta_z(0,z)$ (crosses) corresponding to the surface of a lens with f= 130 cm. The solid lines are linear best fits.
b) Surface profile of the lens. Nx=64 Nz=32 Sweep size Lx=Lz=1.2cm.

Fig.24.a) Temperature distribution inside plexiglass cell obtained with $N_x=64, N_z=32$.
b) $\partial T_r(0,z)/\partial z$ obtained from measurement (triangles) and fitting the data with derivative of Eqn.30 (Solid line).

Fig.25.Temperature distribution measured at different time during the onset of convection in a fluid layer with a free surface heated from below. The depth of fluid is 1 cm. and final temperature difference across layer is 4.5° c whereas the critical

temperature for the onset of convection is 0.3°c. $N_x=64$, $N_z=32$. The time are measured from the switching on of the heat source: (a), (b), (c), (d) correspond to 2,9,16,29 minutes respectively.

Fig.26.a) Typical spectral response curves for photodetector with and without filter.
b) The general configuration to detect the colour from the visible spectrum.

Fig.27.a) Typical position spectrum for a 4 x 32 mm^2 detector of Am^{241} alpha particles. The solid diagonal line shows positions as measured from the pulse height distribution vrs the true position as determined by the mask. The insert shows the position pulse height distribution for hole number three in detail.
b).(i) "X" mask (ii) Hole pattern.
X - Y position-sensitive detector, X-Y signal ratios displayed on an oscilloscope.

Fig.28.Pulse height spectrum from divider circuit for 4 x 32mm^2 detector irradiated with 40 Mev Oxygen ions. Each peak corresponds to a different oxygen ion charge state as indicated. No mask is used on detector.

Fig.29.Position spectrum for a 4 x 32mm^2 detector mounted at the focal plane of a charged particle magnetic spectrometre. The Three groups arise from 12 Mev protons elastically and inelastically scattered from a Yb^{171} target. The measured position resolution reflects the energy resolution as well.

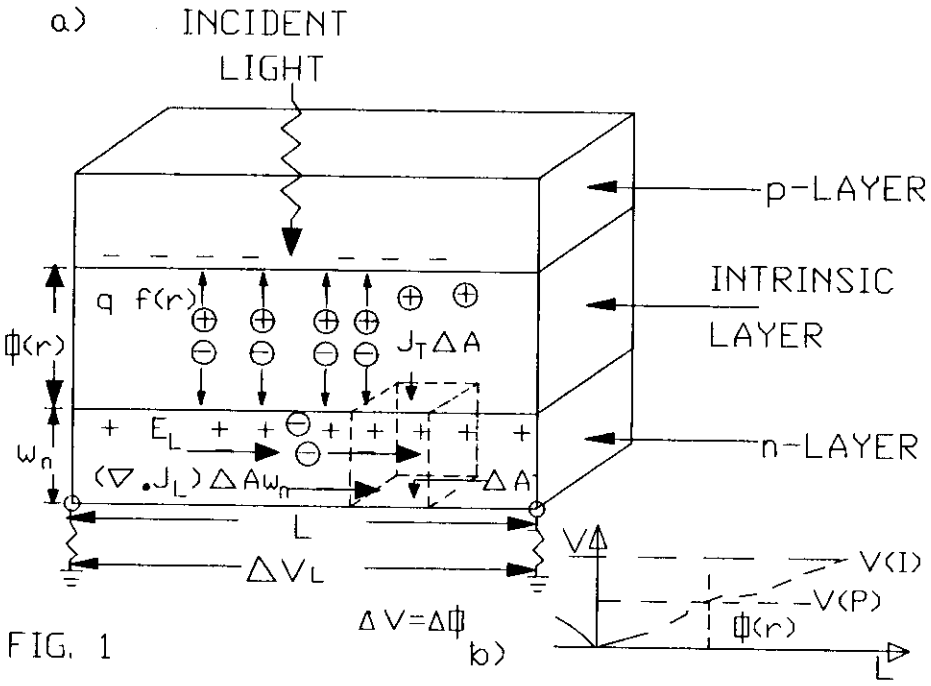

FIG. 1

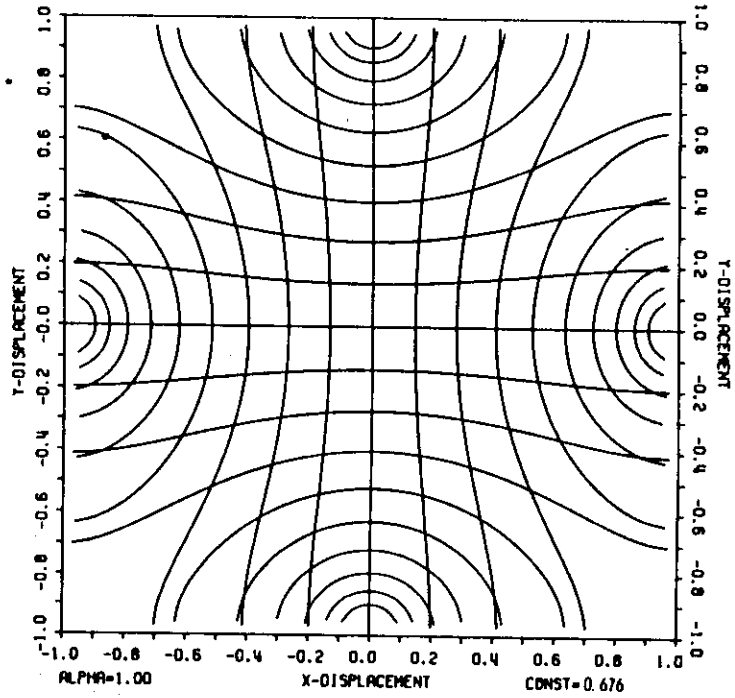

FIG.3

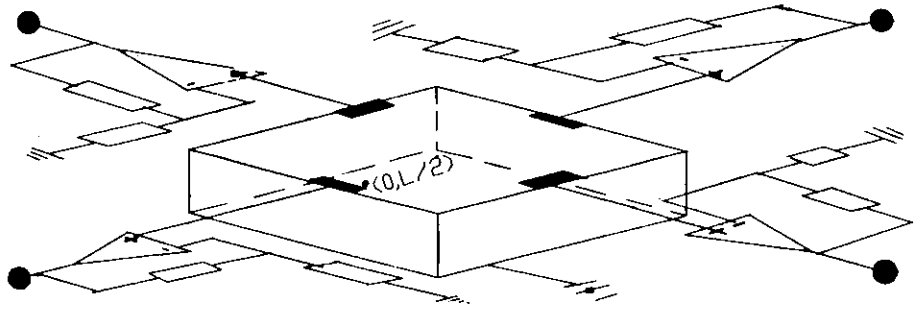

FIG. 2

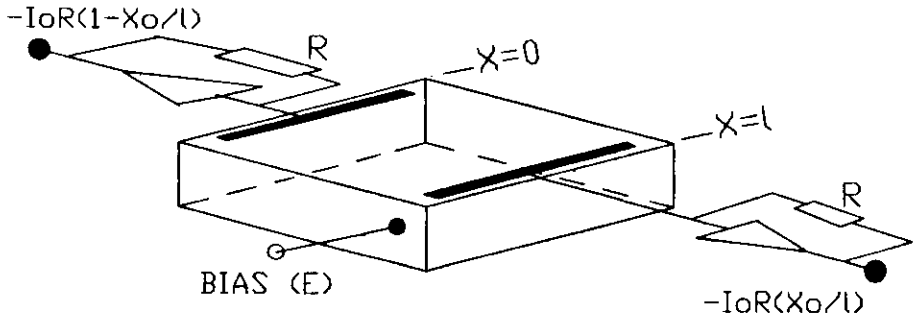

FIG. 4

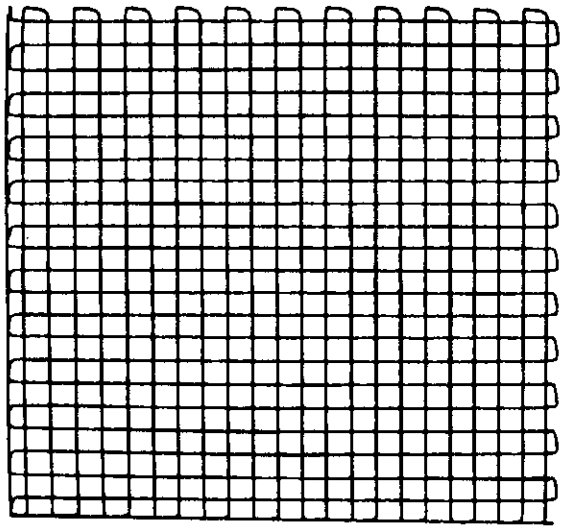

FIG. 5

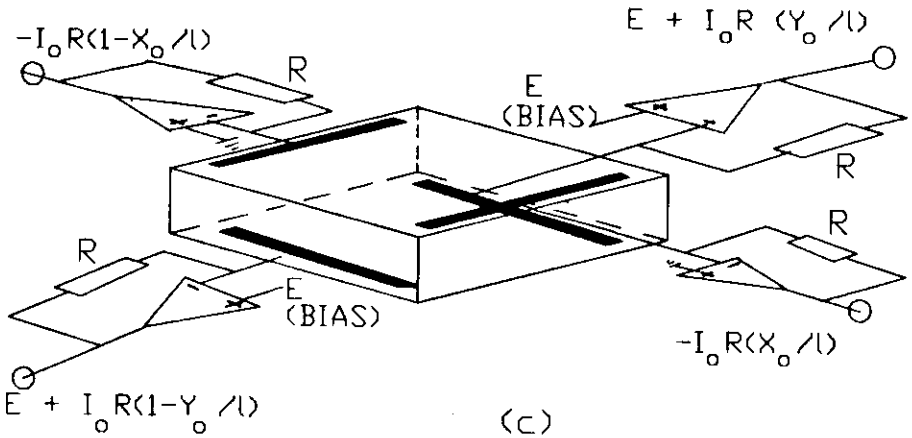

FIG. 5

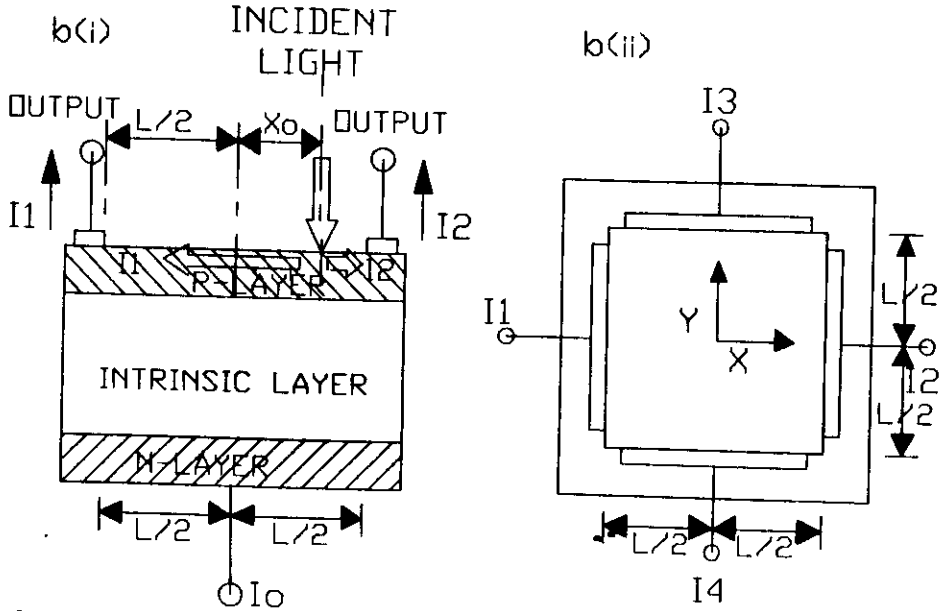

PHOTOCURRENT Io = I1 + I2

FIG. 5

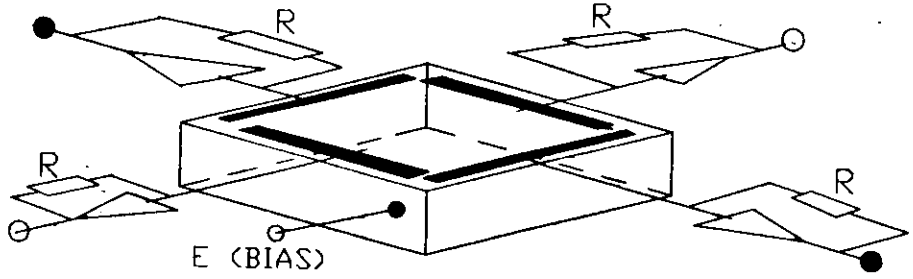

FIG. 6

a

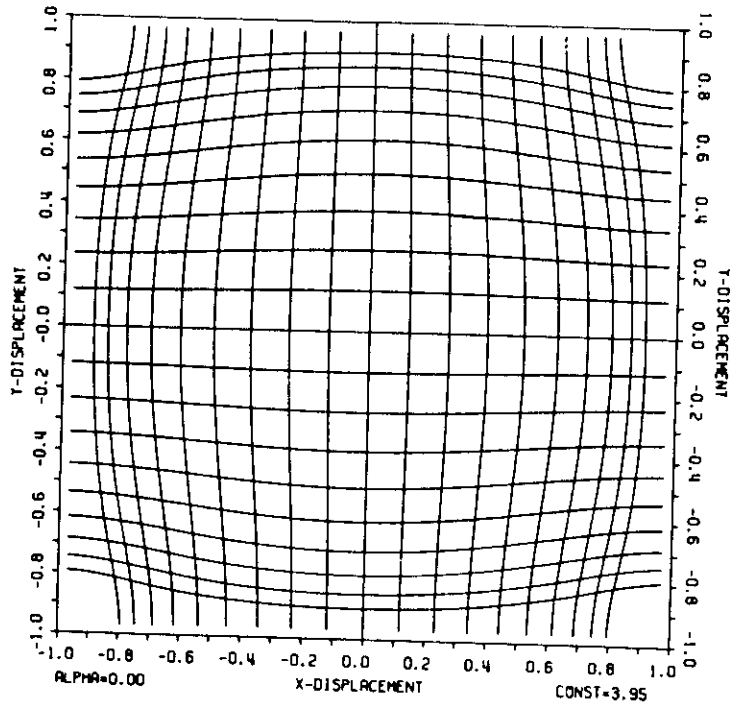

b

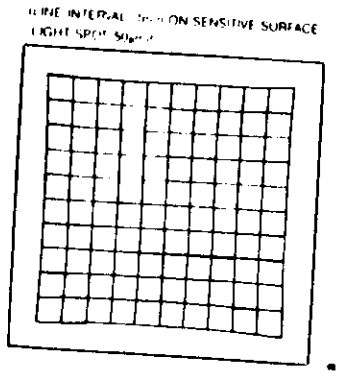

FIG.7

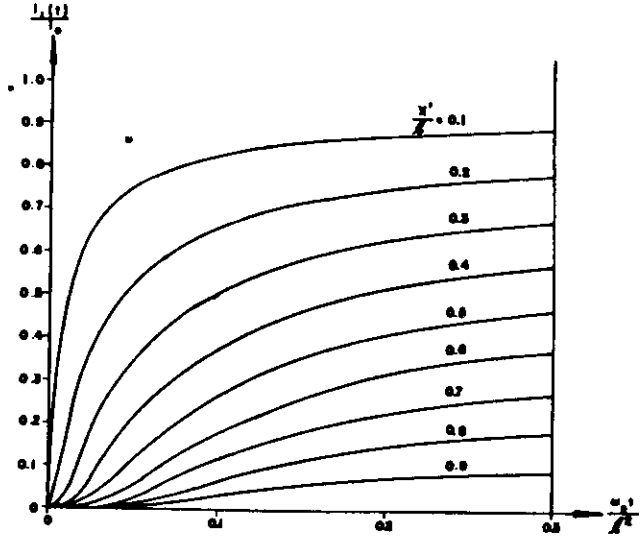

FIG.8

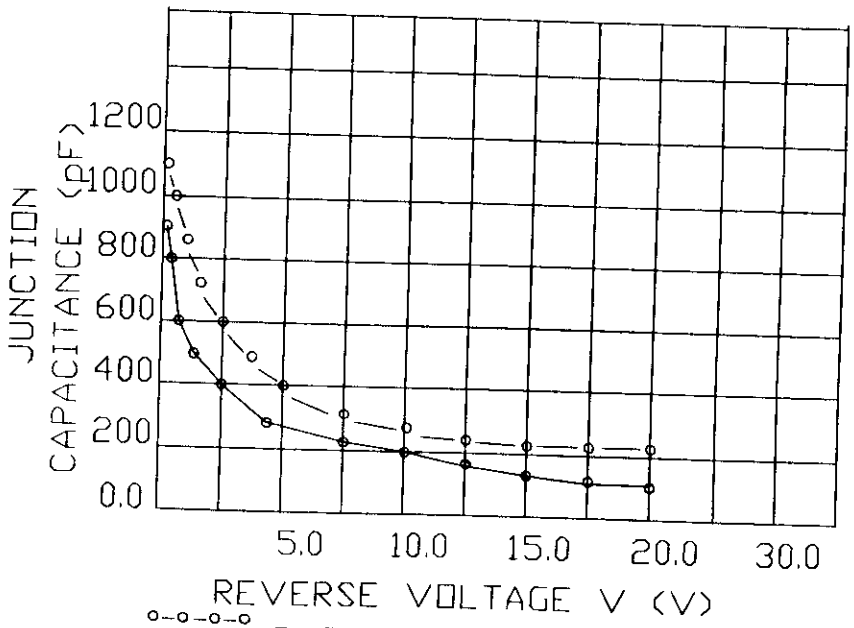

FIG. 9

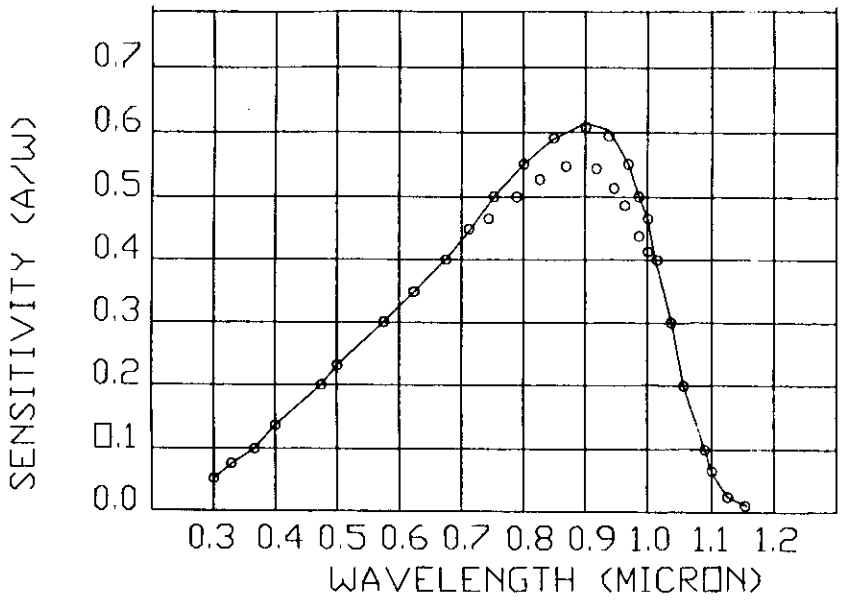

FIG. 10 ° ° ° ° DUO-LATERAL TYPE RESPONSE

o-o-o-o TETRA-LATERAL TYPE RESPONSE

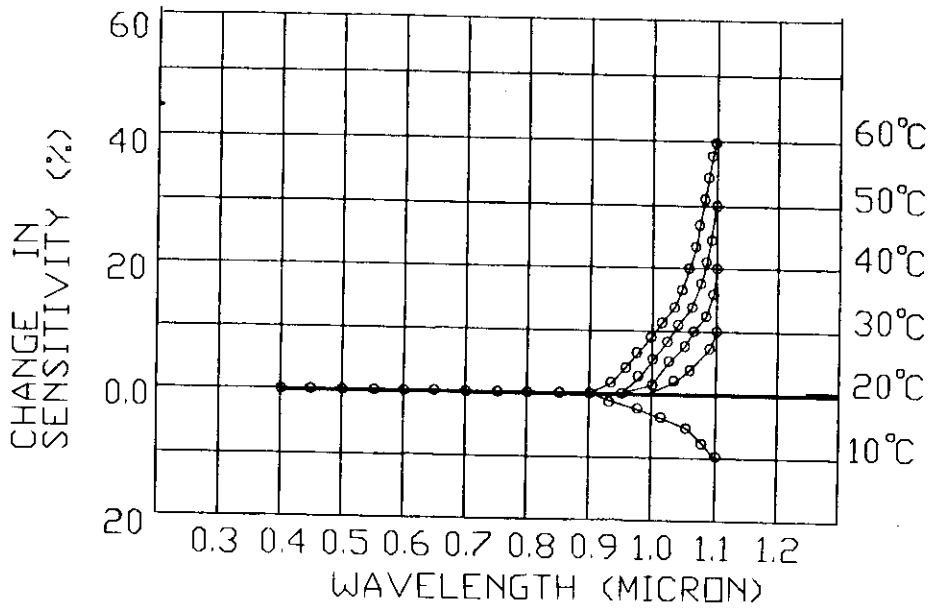

o-o-o-o TETRA-LATERAL, PIN-CUSHION TYPE

FIG.11

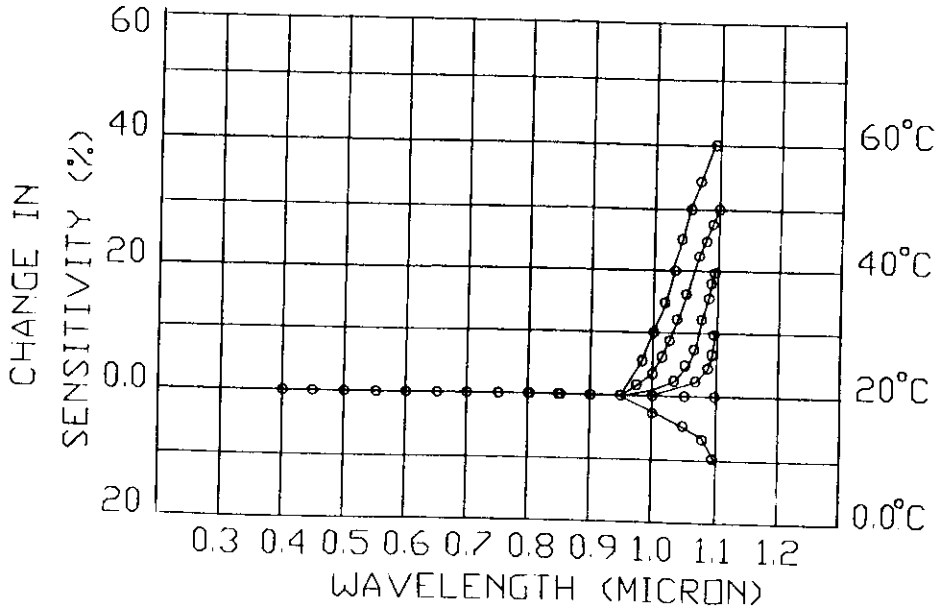

o-o-o-o DUO-LATERAL TYPE RESPONSE

FIG. 11

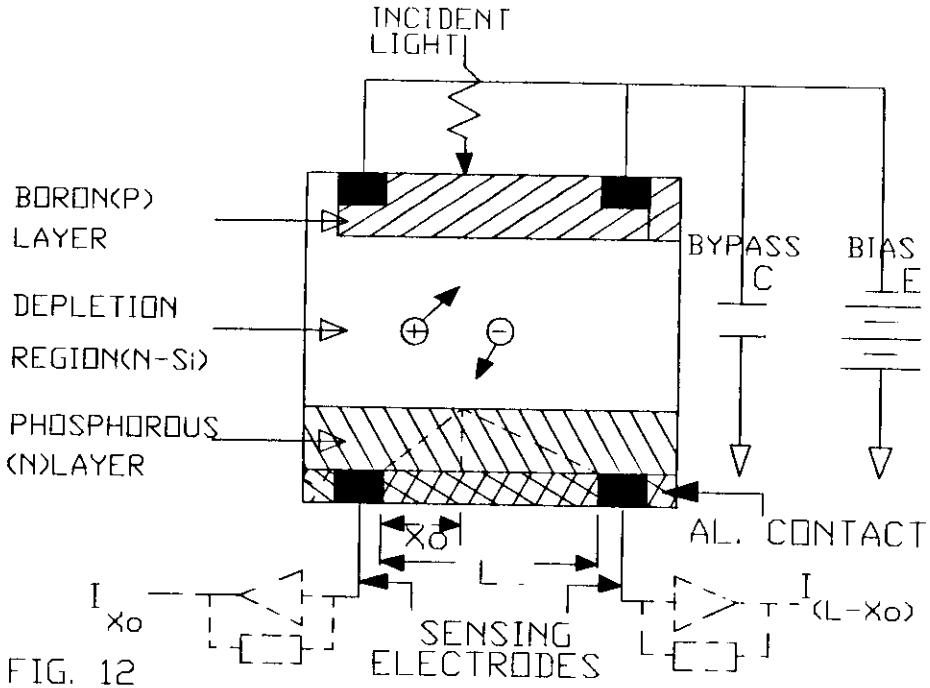

FIG. 12

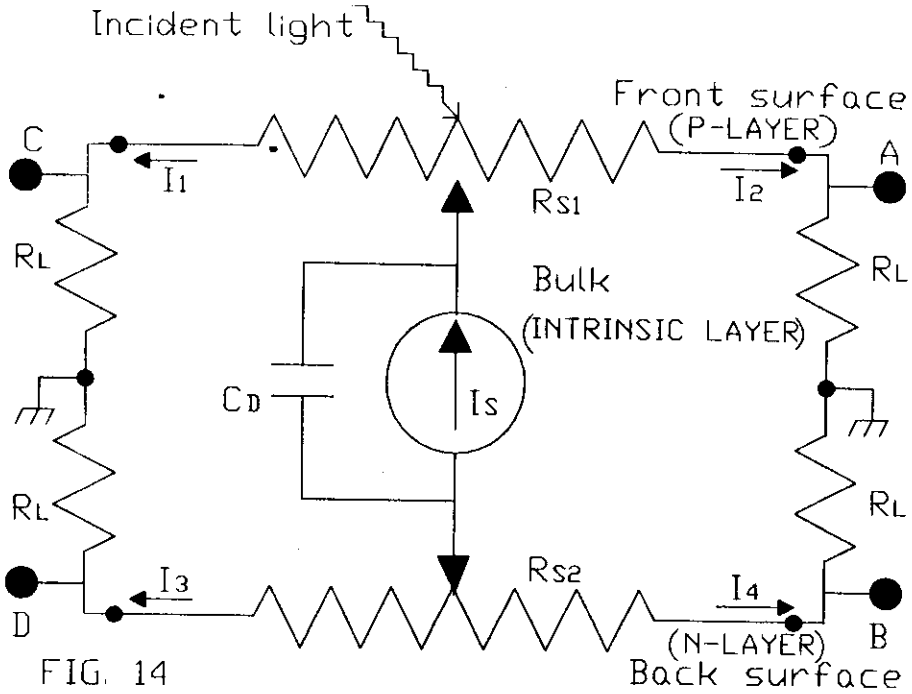

FIG. 14

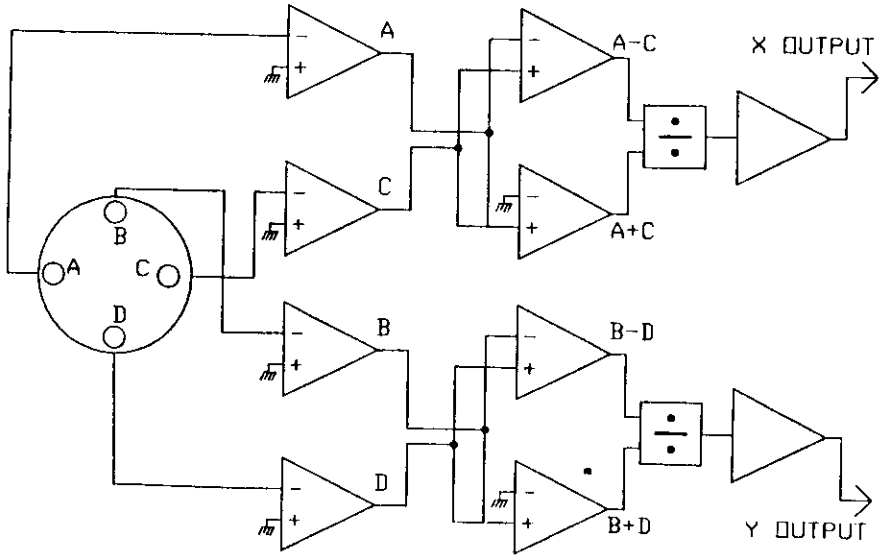

FIG. 13

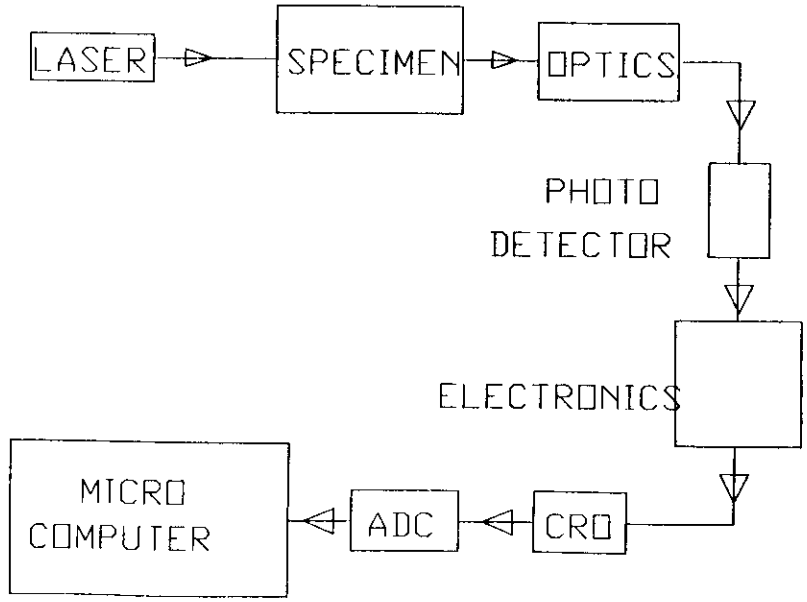

FIG. 15

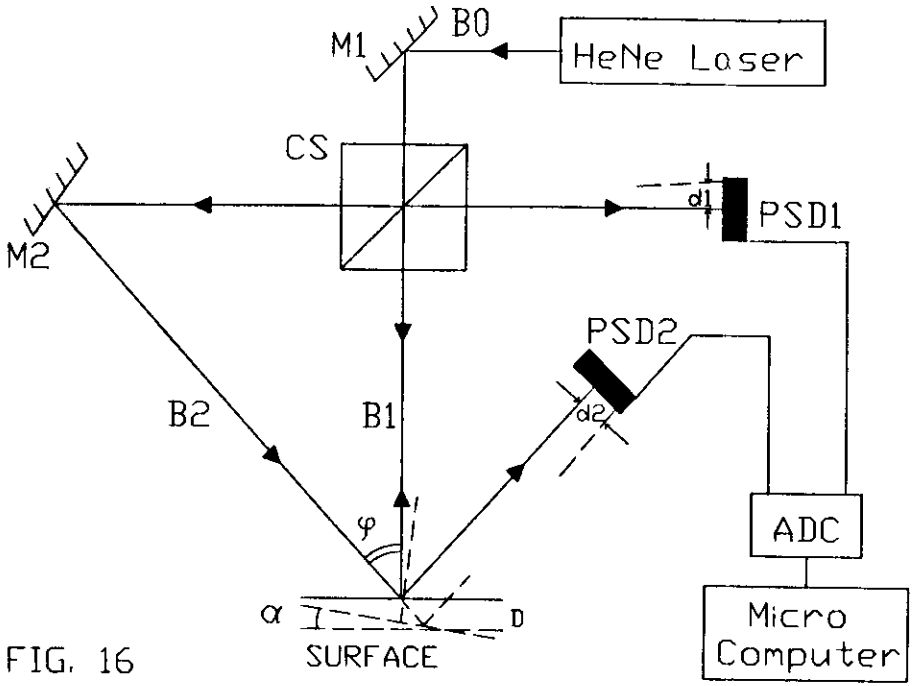

FIG. 16

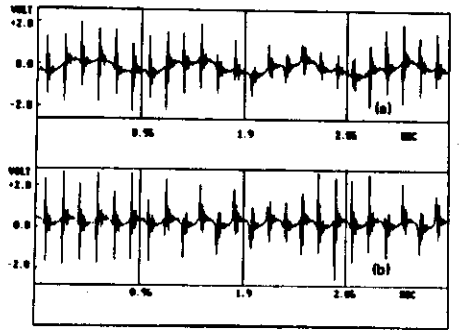

FIG. 18

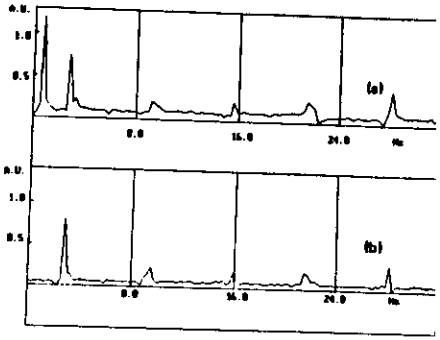

FIG. 19

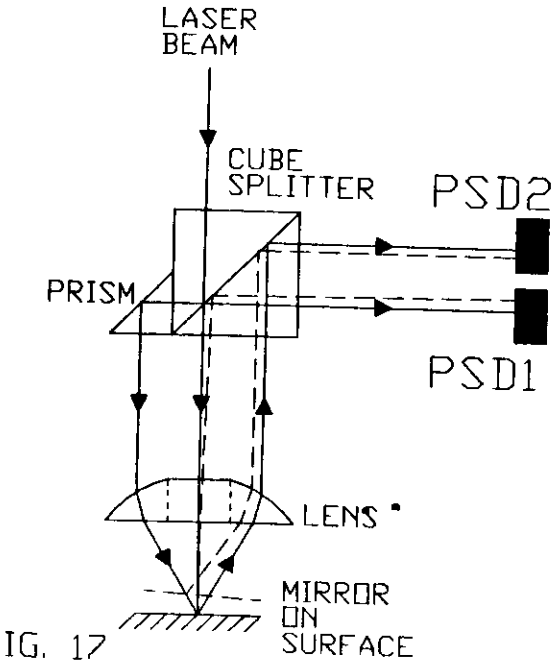

FIG. 17

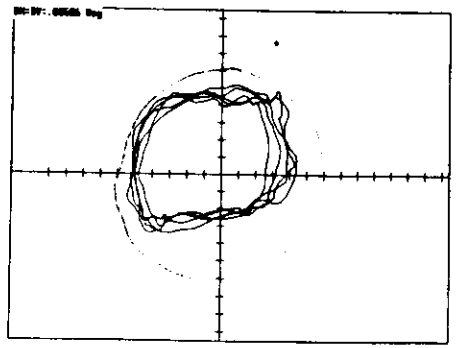

FIG.20

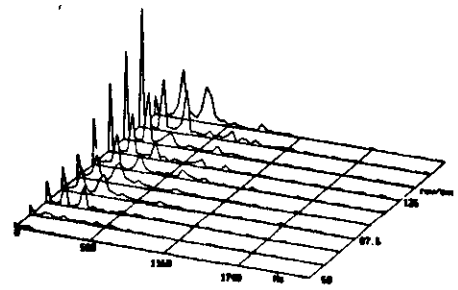

FIG. 21

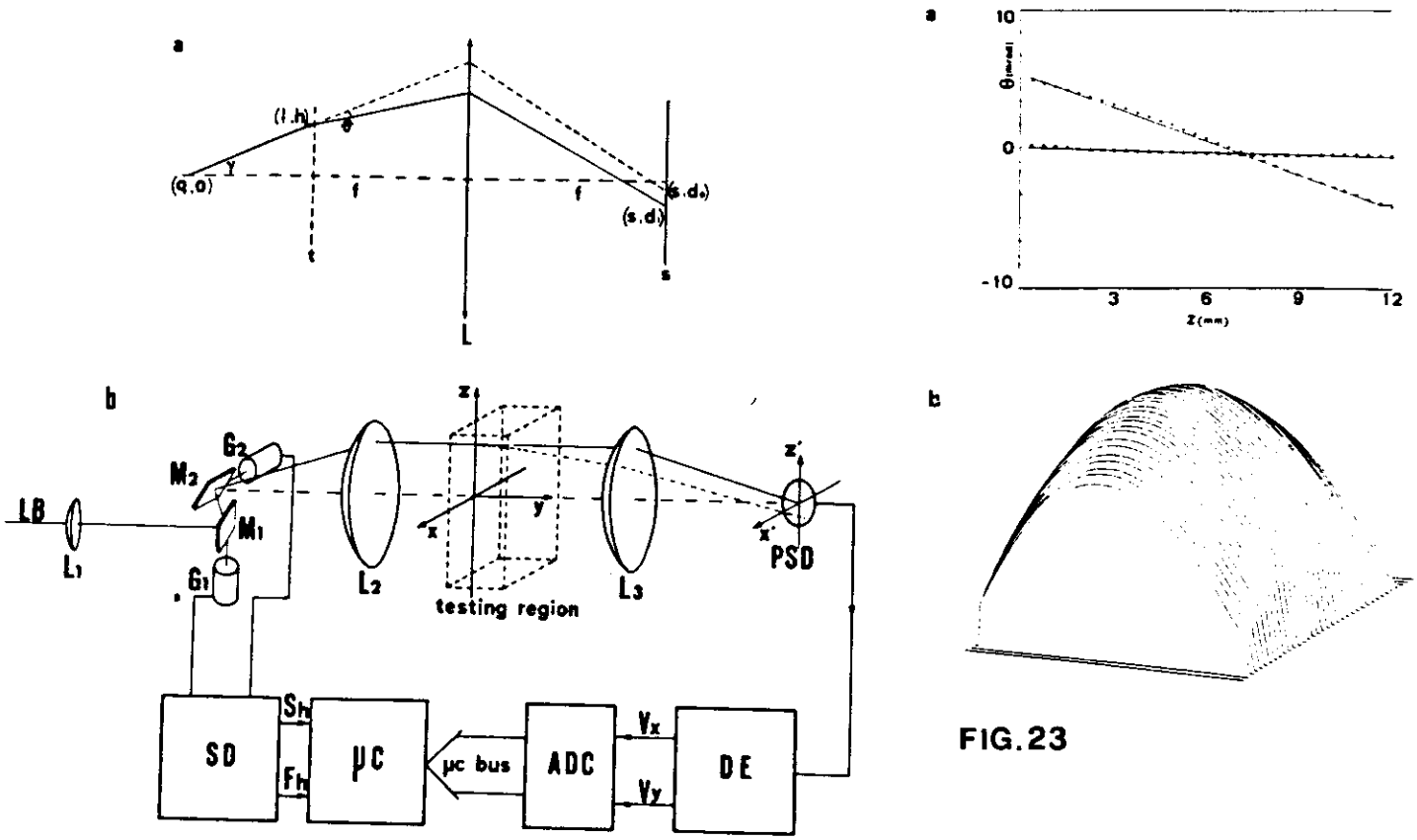

FIG. 22

FIG. 23

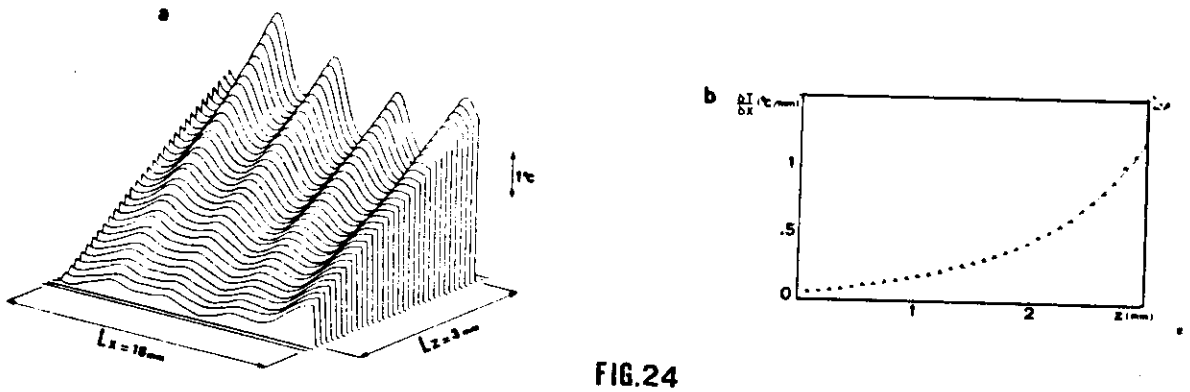

FIG. 24

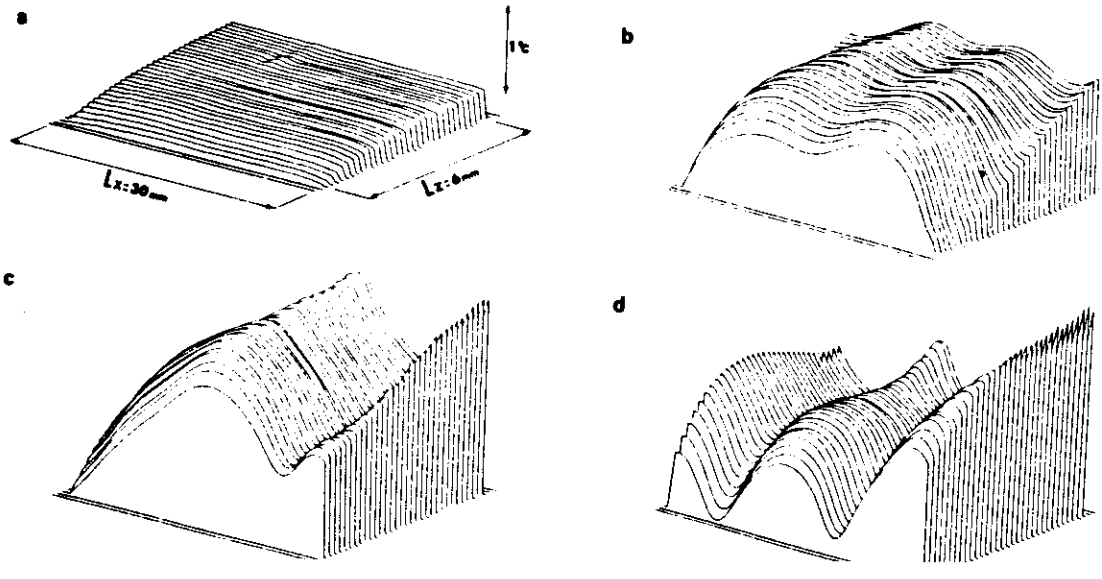

a

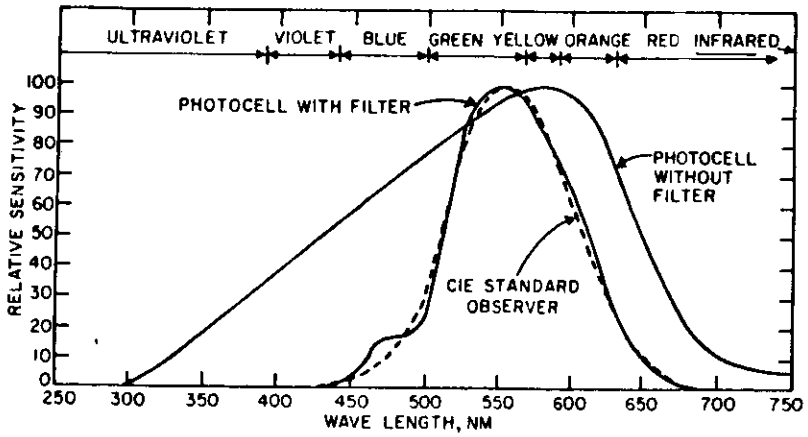

b

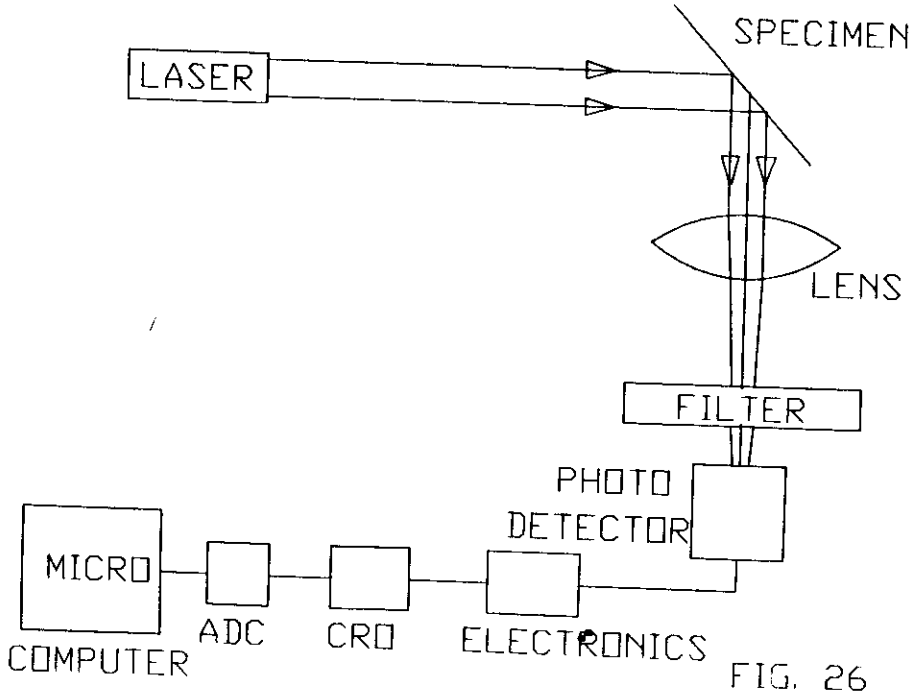

FIG. 26

a

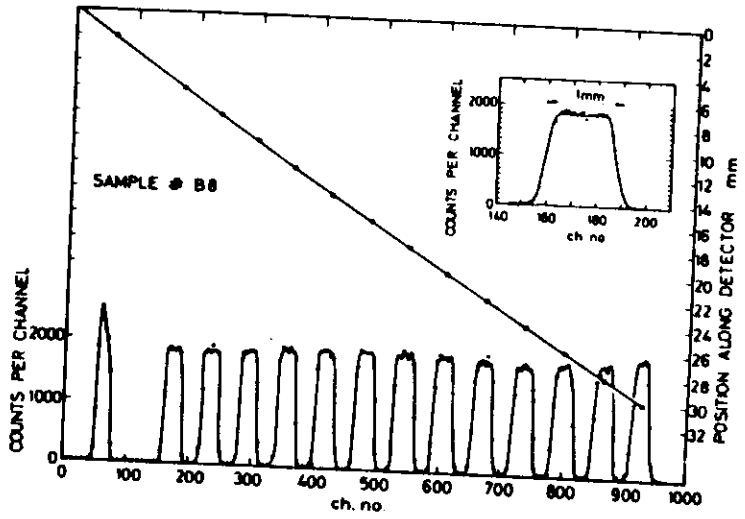

b

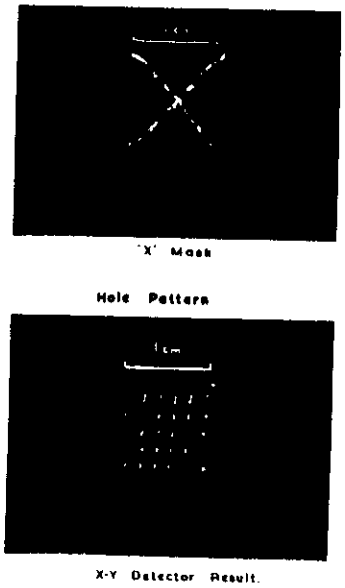

FIG.27

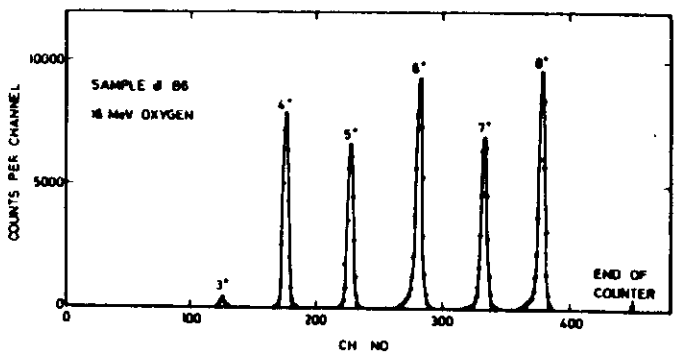
SAMPLE # 86
16 MeV OXYGEN
COUNTS PER CHANNEL
CH NO
END OF COUNTER

FIG. 28

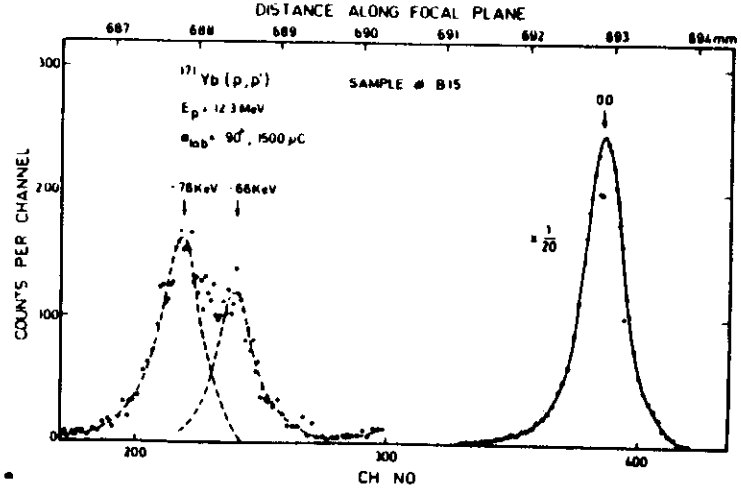
DISTANCE ALONG FOCAL PLANE
SAMPLE # B15
COUNTS PER CHANNEL
CH NO

FIG. 29

CORRECTIONS TO LECTURE NOTES OF BUAH-BASSUAH. P. K.

insert this bracket.

Pg 8 Eqn 9. $\left(\left(1 - \exp\left(\alpha^2 l^2 + (m^2+n^2)\pi^2\right) t/\beta l^2\right)\right)$

Line 2. of 2.3.1 $(\psi = \varphi = \pi/2)$

Pg 11 ~~Replace~~ correct in line 5 Eqn (14) by Eqn (13e)
Eqn (15) by Eqn (13h)

Pg 12 In Eqn 14. in exponent expression write thus $\exp\left[-(a_n^2 + m^2\pi^2)\, t/\beta l^2\right]$
and $a_n^2 = (\alpha^2 l^2 + (2n-1)^2 \pi^2)$

Pg 13 line 9 tetra-lateral.

Pg 20. in Eqn 20. $d = 2D\sin\varphi + \left(\frac{D\cos 2\varphi}{\cos\varphi} + L\right)\tan 2\alpha.$

Pg 22 Eqn(23) $d_1 - d_0 = \dfrac{\left(s - (s-f)\,l/f\,(1 + \tan^2\gamma)\tan\varphi\right.}{1 + \tan\vartheta\tan\gamma}.$

Pg 24 Eqn(30) $v_x(x,z) = L_\gamma \frac{\partial n}{\partial T}\frac{\partial T}{\partial z}(x,z)$

Pg 23 Eqn(26) $V_x = Ax'$

$V_z = Az'$.